Available online at www.sciencedirect.com

ScienceDirect

Proceedings of the Combustion Institute 36 (2017) 1447–1455

Proceedings of the Combustion Institute

www.elsevier.com/locate/proci

Stabilization of a premixed laminar flame on a rotating cylinder

D. Mejia [a,*], M. Bauerheim [b], P. Xavier [a], B. Ferret [a], L. Selle [a,c], T. Poinsot [a,c]

[a] *UPS; IMFT (Institut de Mécanique des Fluides de Toulouse), Université de Toulouse; INPT, Allée Camille Soula, F-31400 Toulouse, France*

[b] *LMFA, Ecole Centrale de Lyon, 36 Avenue Guy de Collongue, 69130 Ecully, France*

[c] *CNRS, IMFT, Av. C. Soula, F-31400 Toulouse, France*

Received 2 December 2015; accepted 20 June 2016
Available online 2 July 2016

Abstract

This paper investigates the stabilization of a laminar premixed flame on a rotating cylinder. Experiments and DNS are combined to analyze the effects of rotation rate on the flow topology and flame stabilization. Both experiment and simulation reveal that the usual stabilization pattern (two symmetric flame roots on both sides of the cylinder) is strongly affected by rotation. The flame roots position on the upper and lower sides of the cylinder are modified with increasing rotation speeds. One of the two flame roots is quenched over a long region. The distance between the flame roots and the flameholder changes with the rotation speed until a bifurcation takes place: at a critical rotation speed, the flame roots merge, and the flame stabilizes upstream of the cylinder. DNS results are used to explain the flame topologies observed experimentally.

Keywords: Laminar flame; Experimental combustion; DNS; Rotating cylinder

1. Introduction

Flow dynamics behind rotating cylinders [1,2] is a classical topic in non reacting flows, where rotation can promote or mitigate hydrodynamic instabilities [3,4]. Flames stabilized behind rotating cylinders (FSBRC) have been much less studied. Nevertheless, FSBRC configurations (Fig. 1) have practical and theoretical interests: (1) New engine concepts, such as wave rotors [5] or constant-volume combustion chambers [6], are currently developed to increase combustion efficiency and reduce pollutant emissions of modern gas turbines. They involve rotating valves, which intermittently open/close the combustion chamber inlet and outlet. These situations may lead to flames which anchor on these valves, and are pulled by them into the feeding chamber, leading to flashback.

(2) From a fundamental point of view, FSBRC constitute a configuration which challenges our understanding of flame/wall interaction and flame stabilization. In a FSBRC (*cf.* Fig. 1), the flame

* Corresponding author. Fax: +33 5 34 32 29 91.
E-mail address: dmejia@imft.fr (D. Mejia).

http://dx.doi.org/10.1016/j.proci.2016.06.138
1540-7489

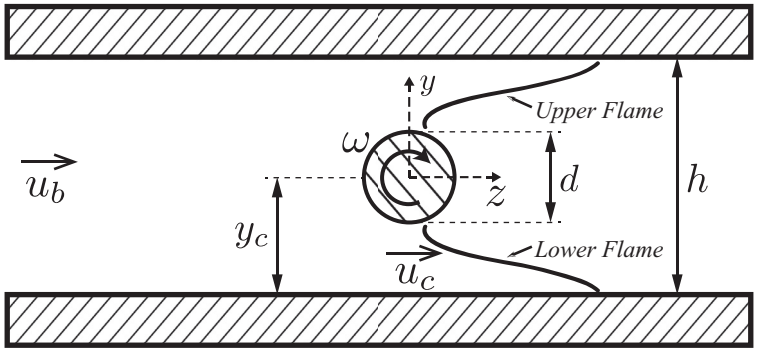

Fig. 1. Sketch of the Intrigs configuration with the parameters controlling the flow topology.

root at the upper side of the cylinder has to stabilize in a boundary layer flow which pushes it downstream, while the flame root located on the lower side is pulled upstream by the cylinder movement. The flame roots (the points where the flame anchors near the cylinder) control not only the mean flame position, but also its dynamics as shown recently for laminar [7–9] and turbulent flames [10].

(3) Introducing rotation in the configuration of Fig. 1 has another effect: it breaks the symmetry of the flow. Symmetry breaking controls the dynamics of many non-reacting flows [11] as well as combustion instabilities [12], so that rotating flame holders may be useful for combustion instabilities control. To describe FSBRCs, it is useful to recall results obtained for non-reacting cases where the flow behind a rotating cylinder is controlled by (1) the Reynolds number $\mathrm{Re} = u_b d/\nu$, (2) the rotation rate $\alpha = \omega d/(2u_b)$, (3) the blockage ratio $\theta = d/h$ and (4) the eccentricity $\gamma = (y_c - h/2)/(0.5(h-d)) = (2y_c/h - 1)/(1-\theta)$. For a fixed unconfined cylinder at zero eccentricity ($\omega = 0$ and $\gamma = 0$), when a critical Reynolds number, $\mathrm{Re}^c \approx 40$, is exceeded, vortices are shed behind the cylinder. For a confined cylinder, the critical Reynolds number depends on the blockage ratio [13]. However, when the cylinder is rotating, the Von Karmann street remains only at low rotation rates ($\alpha < 2$), and is inhibited at larger rotation rates ($2 < \alpha < 4$). For the present study, only flame-holders located at the center of a straight channel will be considered, *i.e.* $\gamma = 0$.

The situation becomes more complex in reactive conditions since the flame can couple with the vortical flow. Cha and Sohrab [14] studied such a case where the rotational axis is normal to the flame front. They showed that rotation enhances the premixed flame stabilization (blow-off and flashback limits). However, no reactive case has been studied where the rotation axis is aligned with the flame.

This paper describes an experimental investigation of the stabilization of a 2D lean premixed methane–air flame on a rotating cylinder for $0 < \alpha < 5$, at moderate blockage ratio ($\theta = 0.235$) and without eccentricity ($\gamma = 0$). Two-dimensional Direct Numerical Simulations (DNS) are also performed to analyze the flame topology and quenching, depending on the rotation rate α. For a fixed cylinder ($\alpha = 0$), a classical stabilization mechanism is observed. For low rotation rates ($\alpha < 4$), the symmetry of the flame is broken and two different behaviors are observed for the two branches of the flame. At large rotation rates ($\alpha > 4$), the flame stabilizes upstream of the cylinder. The geometry of the experimental bench is presented in Section 2, and the numerical setup for DNS in Section 3, followed by the experimental results in Section 4. The stabilization mechanisms are presented and discussed in Section 5.

2. Configuration

The experimental bench is presented in Fig. 2: a lean premixed laminar methane–air flame is stabilized in the wake of a $d = 8$ mm stainless steel rotating cylinder. The cylinder has been grinded and the rugosity is less than 1 μm. The burner has a constant cross section of $h = 34$ mm by $l = 94$ mm. The reactants are premixed in a one-meter long injection tube and equally distributed to six injectors placed at the bottom of the injection chamber. The flow is laminarized by an array of small glass balls and two honeycomb panels and passes through the cooled plenum to ensure a constant fresh-gases temperature. Finally, it enters the combustion chamber where the cylinder is located. The rotating cylinder is placed in a sealed-bearing cage and driven by a brushless electric DC motor. The engine speed ranges from 600 to 20,000 rpm. The combustion chamber has one optical access at the front, and one on each lateral sides. In this study, only one operating point was considered: $\Phi = 0.75$ and $u_b = 1.07\ \mathrm{m.s^{-1}}$. The associated laminar flame speed and adiabatic temperature are $s_l^0 = 0.23$ m/s and $T_{ad} = 1950$ K. For this operating point and for

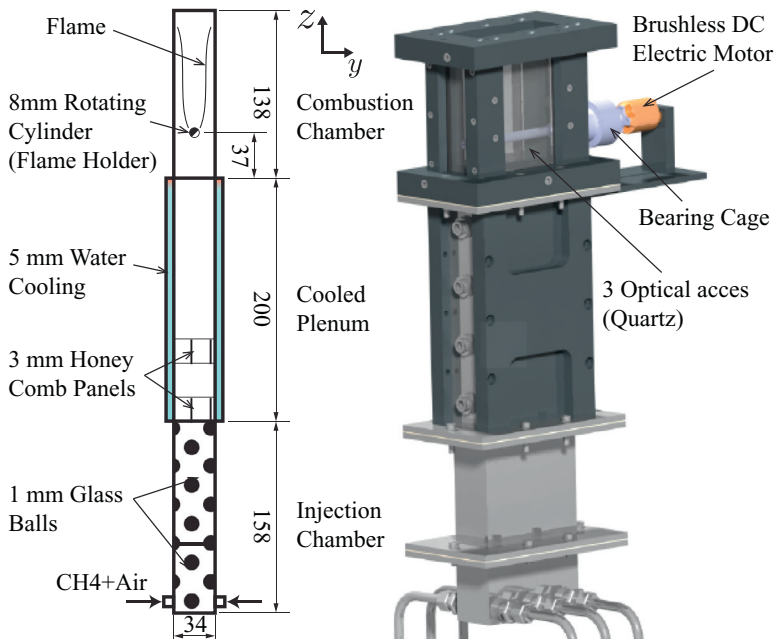

Fig. 2. Transverse cut (*left*) and isometric view (*right*) of the Intrigs burner.

a fixed cylinder ($\alpha = 0$), the flame is steady. Flames are imaged on an intensified PCO-Sensicam camera equipped with a CH* narrow band-pass filter and a *f*/16 180 mm telecentric lens [15]. The camera axis is aligned with the cylinder centerline axis (x).

3. Numerical setup

To analyze experimental results, a DNS was also performed. The compressible code AVBP is used to solve the multi-species Navier–Stokes equations with realistic thermochemistry on unstructured meshes [16]. Numerics are based on a two-step Taylor–Galerkin finite-element scheme called TTG4A, which is third-order in space and fourth-order in time. A two-step mechanism for methane–air is used containing 6 species, based on the methodology described in [17], where adiabatic temperature and laminar flame speed have been validated against a detailed chemical scheme. Schmidt and Prandtl numbers are assumed constant. The NSCBC approach [18] is used to impose acoustic boundary conditions [19] at the inlet (imposed velocity $u' = 0$) and outlet boundary (imposed pressure with a length correction, $p' = 0$). Side walls are treated as no-slip with a heat flux, $\varphi_w = (T - T_w^{side})/R_w$, corresponding to an imposed wall temperature, $T_w^{side} = 300$ K and a heat resistance, $R_w = 10^{-2}$ K.m^2/W. Heat losses are also applied on the rotating cylinder, with the material temperature obtained from the experiment: $T_w^{cyl} = 610$ K. The rotation is accounted for by imposing a velocity $\vec{u}(\theta) = \alpha u_b \vec{e}_\theta$ at the surface of the cylinder. The simulation is performed in a 2D slice that starts at the inlet of the plenum and ends at the chamber outlet. It contains 1.7 million cells, with a minimum cells size of 100 μm and 5 cells in the flame front.

4. Experimental results

First, the global effect of rotation on the flame topology is studied by using several rotation rates from $\alpha = 0$ to 5. The flame is first ignited at $\alpha = 0$. Once thermal equilibrium is reached, the rotation rate is increased in small steps. Three different flame topologies can be identified in Fig. 3: for a fixed cylinder ($\alpha = 0$, Fig. 3 *top*) the flame is stationary and symmetric: this flame shape is referred to as Symmetric Stabilized Downstream (SSD). For low rotation rates ($\alpha < 4$, Fig. 3, *center*) the flame stabilizes downstream of the rotating cylinder, and experiences a strong dissymmetry: the upper flame root moves clockwise along the cylinder, but remains closely attached. The lower flame root is almost quenched and the flame starts producing a noticeable level of CH* emission only far downstream of the cylinder. This flame topology is referred to as Asymmetric Stabilized Downstream (ASD). For larger rotation rates ($\alpha > 4$, Fig. 3 *bottom*), a transition takes place and the flame moves upstream of the rotating cylinder: this situation is named

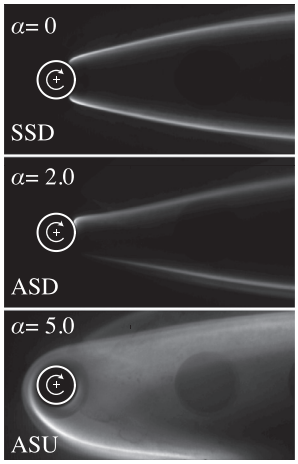

Fig. 3. The three FSBRC topologies observed experimentally: Symmetric Stabilized Downstream flame (SSD, *top*), Asymmetric Stabilized Downstream flame (ASD, *center*), and Asymmetric Stabilized Upstream flame (ASU, *bottom*).

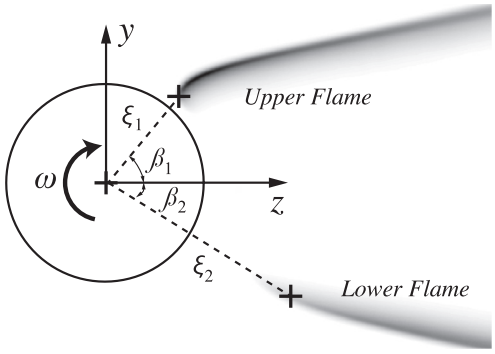

Fig. 4. Sketch of the ASD type flame with the parameters describing the flame topology.

Asymmetric Stabilized Upstream (ASU). In this configuration, the flame roots have merged and it is a new stabilization regime where the velocity profiles and the vortex generation are completely different from the classical stabilization downstream of a bluff-body.

The critical rotation rate at which the flame transitions from ASD to ASU is called α^*. Tests show that α^* is governed by the ratio u_b/s_l^0. More than 100 rotation rates have been tested, from $\alpha = 0$ to 5, leading to flame topologies similar to Fig. 3. In the present experiment, the flame transitions from ASU to ASD in a narrow range: $3.98 < \alpha^* < 4.15$.

When the flame is stabilized downstream, its topology can be described by the two flame roots positions. In order to study the effect of α, the polar coordinates of the roots are defined in Fig. 4: β is the angle between the z axis and the flame root, and ξ, the distance to the center of the cylinder. The upper and lower roots are identified with subscripts 1 and 2, respectively. In the experimental images, the flame root is defined as the location where the gradient of light intensity (measured through CH* emission) is maximum [9,20,21]. Figure 5 shows the evolutions of the roots location versus α for the upper and lower flames. Each curve corresponds to the mean value of four different tests performed on different days. The corresponding error bar is the standard deviation between the four experiments. Snapshots of the flame shapes are shown in Fig. 6, to be compared with DNS results in Section 5. Regarding the upper flame, ξ_1 is almost constant meaning that the flame is always anchored to the cylinder. However, its angle β_1, consistently decreases when α increases. For low rotations rates ($\alpha < 1.5$), the flame location is unchanged but ξ_1 then decreases rapidly. For large rotation rates ($\alpha > 3.2$), the upper flame is actually anchored on the lower side of the cylinder: the flame root is dragged in the direction of the cylinder rotation. The lower flame exhibits a very distinct behavior (Fig. 5): its anchoring angle is less affected by the rotation while its distance to the cylinder varies drastically. ξ_2 increases rapidly until a maximum value of $1.5d$ at $\alpha \approx 1.3$. With a further increase of the rotation rate, the flame almost reattaches to the cylinder, before transitioning to an ASU type flame. One may question the existence of a flame between the cylinder and the root defined as the location of maximum gradient of CH* intensity. However, its emission level being orders of magnitude lower than the remainder of the flame front, it is not considered as a flame front. It is worth noting that for nonzero values of α, the upper flame is more intense than the lower flame. This result suggests that the reactants are mainly consumed by the upper flame.

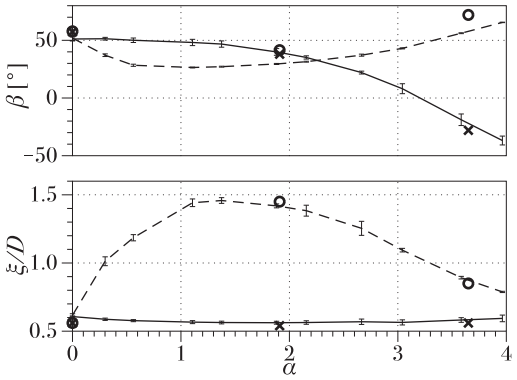

Fig. 5. Flame root angles β (*top*) and distances ξ (*bottom*) function of the rotating rate α. (——-) upper flame, (- - - - -) lower flame (see Fig. 4 for angle and distance definitions). DNS results from Section 5 are presented as × for the upper flame and ◯ for the lower flame.

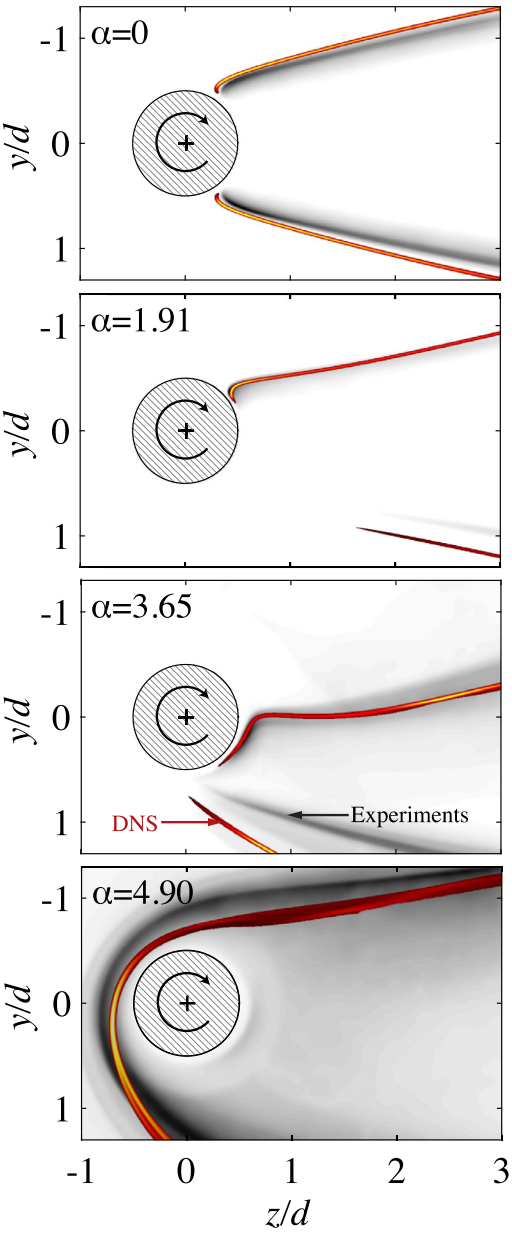

Fig. 6. Snapshots of normalized CH* flame emission and normalized DNS heat release rate fields, for four different rotation rates: $\alpha = 0$, 1.91, 3.65, and 4.90.

This mechanism will be addressed in more details in Section 5.

5. DNS analysis of the ASD quenched flame

In the ASD state, where the two flame roots remain distinct, the results of Figs. 5 and 6 raise multiple questions because the flame structures evidenced in all previous images are very different from usual laminar flames. The most important issue is to identify the mechanisms that may lead to the flame root structures observed on the upper and lower branches. Flame stretch, dilution of the unburnt gases by the burnt gases and heat losses to the cylinder are the three obvious phenomena that may explain these structures. At low rotation rates, the lower branch quenching distance is much larger than usual. Such a quenched zone can be explained either by an excessive stretch, dilution or heat loss (or a combination of the three). These questions are now addressed via numerical simulation. DNS were performed for various rotation rates and essentially produced the same results as the experiment. Figure 6 presents the flame topology obtained by DNS corresponding to the experimental results. The agreement is good, β and ξ are well predicted (*c.f.* Fig. 5). In particular, quenching in ASD flames for moderate rotation rates, and upstream flame stabilization for higher rotation speeds, are well captured. Nevertheless, discrepancies are observed for $\alpha = 1.91$ and 3.65: while the upper flame is well described, the lower flame have the correct distance ξ_2 but not the right angle β_2 ($\beta_2^{DNS} = 72°$ while $\beta_2^{EXP} = 56°$, at $\alpha = 3.65$). This discrepancy may come from the reduced kinetic mechanism used in the DNS or the inability of the CH* chemiluminescence to capture local flame extinctions [22].

Once validated, the DNS can be used for detailed diagnostics, using quantities virtually impossible to quantify experimentally. Here, the analysis is limited to the quenched branch of the two flame roots at $\alpha = 1.91$ and 3.65. These two cases have been chosen because they have very different stabilizations. At the lower rotation rate $\alpha = 1.91$, the lower flame is further downstream than the case of higher rotation rate, $\alpha = 3.65$.

5.1. Flame stretch

One mechanism that could explain the quenching of the lower flame branch is stretch. This effect is significant for counterflow flames [23], in particular on flame speed and quenching limits. Figure 7 corresponds to a steady state axial velocity field with the corresponding stream lines. The streamlines show that, for both cases, the rotating cylinder carries burnt gases from the upper flame towards the lower flame branch. The burnt gases coming from the upper flame meet the fresh gases and create a counterflow. The stretch is calculated in transverse plane of the flame front (ζ-direction in Fig. 7), ζ is the curvilinear abscissae defied as the maximum of the heat release rate, or the prolongation of the lower flame front. The stretch κ, is defined as:

$$\kappa(\zeta) = -\vec{\mathbf{n}}\vec{\mathbf{n}} : \nabla \cdot \vec{\mathbf{u}} + s_d(\nabla \cdot \vec{\mathbf{u}}) \quad (1)$$

where $\vec{\mathbf{u}}$ is the velocity field with its axial component u and the vertical component v, $\vec{\mathbf{n}}$ is the direction normal to the flame front and s_d is the displacement

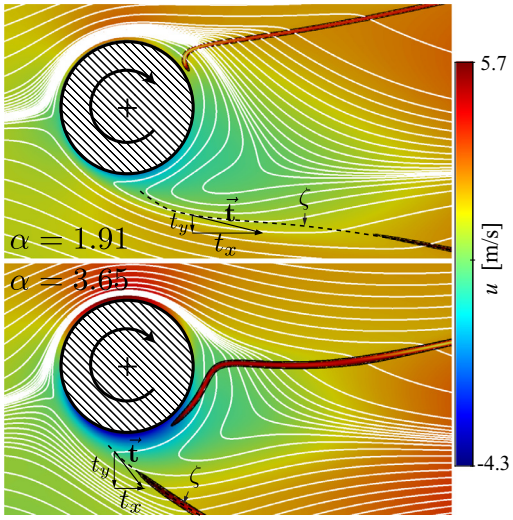

Fig. 7. DNS steady state 2D axial velocity field with the corresponding stream lines for $\alpha = 1.91$ (*top*) and $\alpha = 3.65$ (*bottom*).

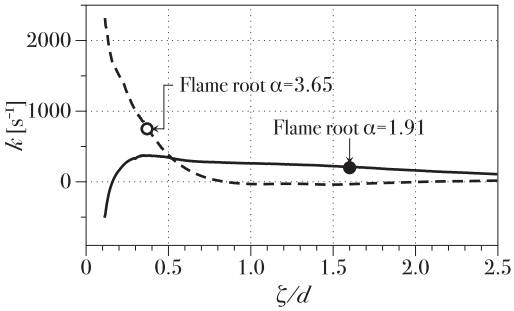

Fig. 8. Stretch, κ, from Eq. (2) along the lower flame abscissa ζ of the lower branch, indicated by a black dashed line in Fig. 7. For both, $\alpha = 1.91$ (——-) and 3.65 (- - - - -). The ζ coordinate of the lower flame root are represented by (◯) for $\alpha = 1.91$ and (•) for $\alpha = 3.65$.

speed. For a stationary flame Eq. (1) becomes:

$$\kappa(\zeta) = \nabla_t \cdot \vec{\mathbf{u}}_t = t_x^2 \frac{\partial u}{\partial x} + t_x t_y \left(\frac{\partial u}{\partial y} + \frac{\partial v}{\partial x} \right) t_y^2 \frac{\partial v}{\partial y} \quad (2)$$

where $\vec{\mathbf{t}}$ is the direction transverse to the flame front, as shown in Fig. 7. The values of stretch from Eq. (2), for both α =1.91 and 3.65, are plotted in Fig. 8. For the low rotation rate, stretch at the lower flame root has a value of $\kappa \approx 250\,\mathrm{s}^{-1}$. The critical stretch for the methane–air flame quenching, at this operating point, is found to be around $\kappa_c = 4000\,\mathrm{s}^{-1}$ [24,25]. Therefore, it is unlikely that stretch is responsible for the flame quenching. Moreover, Fig. 8 also shows that at the higher rotation rate, the flame can withstand stretch levels of 750 s^{-1}, giving further indication that stretch is not likely to be responsible for the local extinction.

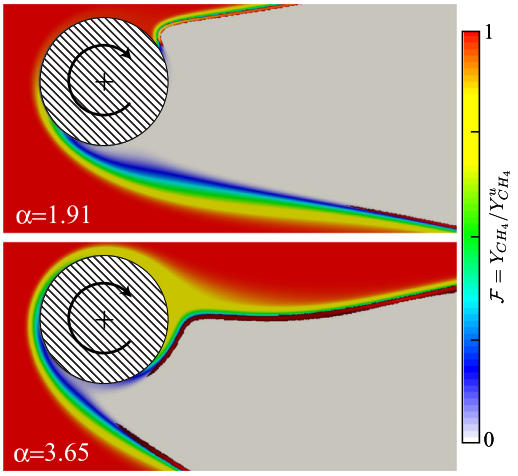

Fig. 9. DNS reduced fuel mass fraction field, $\mathcal{F}$ $\alpha = 1.91$ (*top*) and $\alpha = 3.65$ (*bottom*).

5.2. Dilution

Another aspect that could explain the flame quenching of the lower branch is the dilution of the unburnt gases by the burnt gases. An indicator for the dilution is the reduced fuel mass fraction $\mathcal{F} = Y_{\mathrm{CH_4}}/Y^u_{\mathrm{CH_4}}$, which is based on the initial fuel mass fraction in the unburnt side $Y^u_{\mathrm{CH_4}}$. $\mathcal{F}$ goes from one in the unburnt gases to zero in the burnt gases. A 2D field of the reduced mass fraction is shown in Fig. 9. The rotating cylinder carries burnt gases towards the lower flame branch. These burnt gases impact the unburnt gases and create a stagnation point but not significant dilution is observed. The border between the fresh and burnt gases is clearly seen. On the other hand, for high rotation rates ($\alpha = 3.65$) some of the burnt gases are entrained all the way around the cylinder. This phenomena creates a diluted zone in the unburnt gases of the upper flame where $\mathcal{F} < 1$. It suggests that there exist a critical rotation rate, at which the upper branch burnt gases, make a complete rotation and mix back with the incoming unburnt gases. Unfortunately, this phenomenon does not seem to explain the quenching of the lower branch at low rotation rates.

5.3. Heat losses

The cooling of the burnt gases by the "cold" cylinder could also explain the quenching of the lower branch. The reduced temperature, Θ is displayed in Fig. 10. $\Theta = (T - T^u)/(T^b - T^u)$ is based on the unburnt (T^u) and burnt mixture temperatures ($T^b = T_{ad}$, *i.e.* the adiabatic flame temperature). Θ goes from zero in the unburnt gases to one in the burnt gases. The reduced temperature field shows that the burnt gases carried

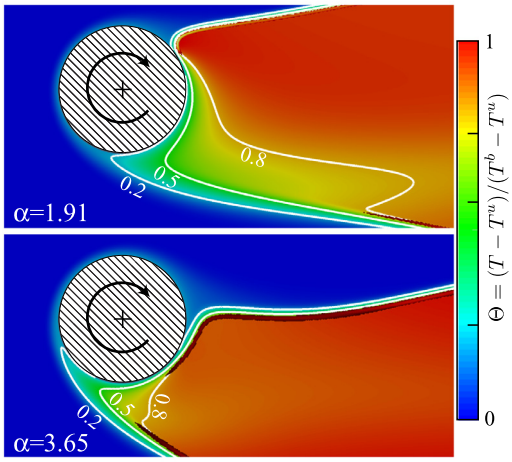

Fig. 10. DNS reduced temperature field obtained for $\alpha = 1.91$ (*top*) and $\alpha = 3.65$ (*bottom*).

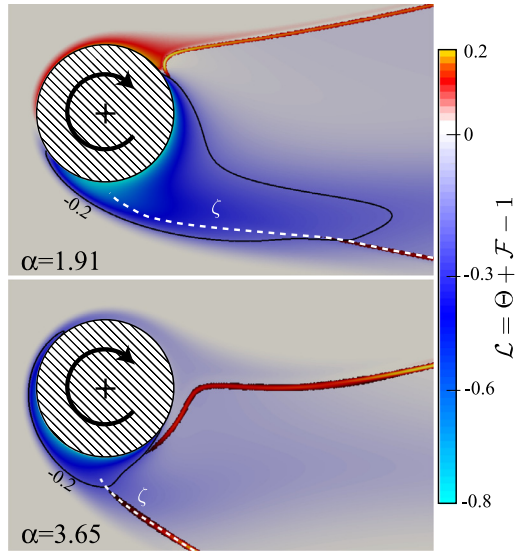

Fig. 11. Entalphy loss field $\mathcal{L} = \Theta + F - 1$, obtained for $\alpha = 1.91$ (*top*) and $\alpha = 3.65$ (*bottom*).

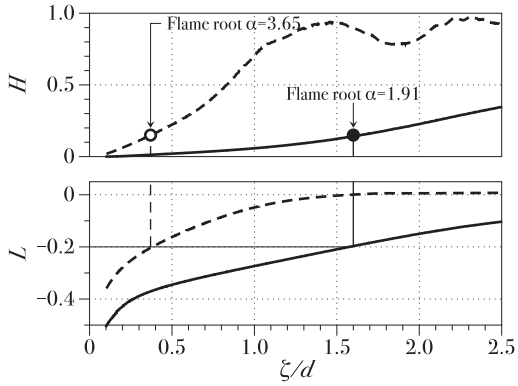

Fig. 12. Reduced heat release rate $\mathcal{H}$ (*top*) and enthalpy losses $\mathcal{L}$ (*bottom*), along the lower flame abscissa ζ of the lower branch, indicated by a white dashed line in Fig. 11. For both, $\alpha = 1.91$ (——) and 3.65 (- - - - -). The ζ coordinates of the lower flame root are represented by (•) for $\alpha = 1.91$ and (◯) for $\alpha = 3.65$.

from the upper flame are cooled as they travel along the "cold" cylinder walls ($T_w^{cyl} = 610$ K). For the low rotation rate ($\alpha = 1.91$) the region of low temperature (less than the adiabatic flame temperature *i.e.* iso-contour $\Theta = 0.8$ in Fig. 10), is bigger than in the case of a higher rotation rate ($\alpha = 3.65$). This region of low temperature may explain why the lower branch is quenched, and it suggests that there is a significantly larger heat flux from the burnt gases to the cylinder at low rotation rates. In the DNS, the cylinder temperature is imposed and constant for all rotation rates. This cylinder temperature, T_w^{cyl}, was measured experimentally for the different rotation rates. The variation of T_w^{cyl} with α is within the uncertainty of the measurements ± 50 °K. An effort has been focused on reducing this experimental uncertainty, as well as the implementation of the joint resolution of combustion and heat transfer in the solid by coupled solvers. However, until now, the reason why the low temperature region is larger at low rotation rates is still not well understood.

5.4. Enthalpy losses

A proper quantity to visualize this effect combining dilution and cooling due to the rotating cylinder, is the enthalpy loss $\mathcal{L}$ [26], defined as:

$$\mathcal{L} = \Theta + \mathcal{F} - 1, \tag{3}$$

For adiabatic cases with a one-step chemistry and a unit Lewis number, $\mathcal{L} = 0$. The field of enthalpy loss $\mathcal{L}$ is shown in Fig. 11 for both cases. As expected, it goes to zero far from the cylinder and side-walls. In the case of $\alpha = 1.91$ enthalpy loss is even slightly larger than zero for the upper flame, where a small heating of the fresh premixed gases (initially at $T^u = 300$ K) takes place near the cylinder. This effect is not seen in the case $\alpha = 3.65$ because at higher rotation rates the burnt gases are dragged upstream of the cylinder (Fig. 9 *bottom*). Therefore, the effect of dilution (reduction of $\mathcal{F}$) overcomes the effect of preheating (increase of Θ). This region of low enthalpy in the upper part of the cylinder explains why the upper flame front is less intense at $\alpha = 3.65$ than at $\alpha = 1.91$.

To quantify the effects due to enthalpy losses on the flame quenching, the reduced heat release rate $\mathcal{H} = HR/HR_{max}$ and the heat losses $\mathcal{L}$, are plotted in Fig. 12, along the curvilinear abscissae ζ of the

lower branch. Enthalpy loss reaches large negative values (−0.8) near the bottom of the rotating cylinder, indicating a massive effect of heat losses for the lower flame. The flame root is defined here as the location of the maximum of the heat-release gradient, this point correspond to a value of $\mathcal{L} \approx -0.2$, for both, $\alpha = 1.91$ and 3.65. When $\mathcal{L}$ reaches values of the order of −0.2, flame quenching cannot be avoided. The lower flame can only start burning when $\mathcal{L}$ increases again downstream of the cylinder. This inert mixture corresponds to the region enveloped by the isocontour −0.2 in Fig. 11. This region is much larger for $\alpha = 1.91$ than it is for $\alpha = 3.65$, which explains why, at low rotation rate, the lower flame is pushed downstream.

Figure 9 showed that little dilution takes place on the lower branch of flame. As a result, this configuration is equivalent to having a 1D counterflow flame, with unburnt gases on one side and burnt gases with reduced enthalpy on the other side. With this analogy, for a given strain rate, if the enthalpy of the burnt gases is reduced to the limit of $\mathcal{L} = -0.2$ there will be flame extinction. The reduction of burnt gases enthalpy is mainly governed by heat losses induced by the "cold" cylinder so that flame quenching is controlled by both rotation rate and heat transfer. The reason why the heat loss to the cylinder is more important for $\alpha = 1.91$ remains unknown, but it is the subject of upcoming studies.

6. Conclusion

This article describes the first study of the stabilization of a lean laminar premixed methane–air flame on a rotating cylinder. For non-reactive flows, the rotation of the cylinder is known to impact the development of instabilities. For reactive flows, both experiment and simulation reveal unusual stabilization patterns, depending on the rotation speed of the cylinder. First, experiments and simulations are performed at several rotation rates. For the upper branch a very good agreement for flow topology and flame shape was found. However, for the lower branch the angle β_2 is not well reproduced by the DNS. This difference is due to the reduced kinetics mechanism used in this study. Computations with more sophisticated kinetic mechanisms will be considered in future studies. For low rotation speeds, flame quenching appears for the lower flame branch. Using DNS results, this quenching is found to be controlled by heat losses: the rotation of the flame-holder carries low enthalpy burnt products from the upper branch to the lower branch, leading to flame quenching. The enthalpy loss, of the dragged burnt products, is mainly due to the heat losses to the cylinder. The reason why the heat loss to the cylinder is more important for low rotation rates remains unknown. However, the joint resolution of combustion and heat transfer in the solid by coupled solvers is underway. This should give a better understanding of the interaction between heat transfer and rotation rate. At higher rotational speeds, a bifurcation appears and the flame stabilizes upstream of the cylinder. Ongoing works are being performed to compare DNS data with experimental velocity fields, and to further understand the ASU stabilization mechanism.

Acknowledgments

The research leading to these results has received funding from the European Research Council under the European Union's Seventh Framework Programme (FP/2007-2013)/ERC Grant Agreement ERC-AdG 319067-INTECOCIS.

References

[1] S. Mittal, B. Kumar, *J. Fluid Mech.* 476 (2003) 303–334.
[2] S. Camarri, F. Giannetti, *J. Fluid Mech.* 642 (2010) 477–487.
[3] J. Guckenheimer, A. Mahalov, *Phys. Rev. Lett.* 68 (1992) 2257.
[4] R. Bourguet, D.L. Jacono, *J. Fluid Mech.* 740 (2013) 342–380.
[5] P. Akbari, R. Nalim, N. Mueller, *J. Eng. Gas Turbines Power* 128 (2006) 717–735.
[6] B. Robic, Constant-Volume Combustion (CVC) Chamber for an Aircraft Turbine Including an Intake/Exhaust Valve Having a Spherical Plug, *patent WO2014020275 A1*, Snecma 2014.
[7] K. Kedia, H. Altay, A. Ghoniem, *Proc. Combust. Inst.* 33 (2011) 1113–1120.
[8] A. Cuquel, D. Durox, T. Schuller, *C. R. Méc.* 341 (2013) 171–180.
[9] D. Mejia, L. Selle, R. Bazile, T. Poinsot, *Proc. Combust. Inst.* 35 (3) (2015) 3201–3208.
[10] M. Bauerheim, G. Staffelbach, N. Worth, J. Dawson, L. Gicquel, T. Poinsot, *Proc. Combust. Inst.* 35 (3) (2015) 3355–3363.
[11] Z. Feng, P. Sethna, *J. Fluid Mech.* 199 (1989) 495–518.
[12] M. Bauerheim, P. Salas, F. Nicoud, T. Poinsot, *J. Fluid Mech.* 760 (2014) 431–465.
[13] M. Sahin, R.G. Owens, *Phys. Fluids* 16 (5) (2004) 1305–1320.
[14] J. Cha, S. Sohrab, *Combust. Flame* 106 (1996) 467–477.
[15] R. Price, I. Hurle, T. Sudgen, *Proc. Combust. Inst.* 12 (1969) 1093–1102.
[16] T. Schönfeld, M. Rudgyard, *AIAA J.* 37 (11) (1999) 1378–1385.
[17] B. Franzelli, E. Riber, M. Sanjosé, T. Poinsot, *Combust. Flame* 157 (7) (2010) 1364–1373.
[18] T. Poinsot, T. Echekki, M.G. Mungal, *Combust. Sci. Technol.* 81 (1–3) (1992) 45–73.
[19] L. Selle, F. Nicoud, T. Poinsot, *AIAA J.* 42 (5) (2004) 958–964.
[20] V. Kornilov, *Dynamics and Nonlinear Thermo-Acoustic Stability Analysis of Premixed Conical Flames*, Technische Universiteit Eindhoven, 2006 Ph.D. thesis.

[21] D. Mejia, *Wall-Temperature Effects on Flame Response to Acoustic Oscillations*, INP Toulouse, 2014 Ph.D. thesis.
[22] H.N. Najm, P.H. Paul, C.J. Mueller, P.S. Wyckoff, *Combust. Flame* 113 (1998) 312–332.
[23] J. Buckmaster, D. Mikolaitis, *Combust. Flame* 47 (1982) 191–204.
[24] B. Coriton, M.D. Smooke, A. Gomez, *Combust. Flame* 157 (11) (2010) 2155–2164.
[25] L. Tay-Wo-Chong, M. Zellhuber, T. Komarek, H.G. Im, W. Polifke, *Flow Turbul. Combust.* (2015) 1–32. Springer. DOI: 10.1007/s10494-015-9679-0.
[26] P. Simon, S. Kalliadasis, J. Merkin, S.K. Scott, *J. Math. Chem.* 31 (3) (2002) 313–332.